Article

# Lattice Dynamics To Trigger Low Temperature Oxygen Mobility in Solid Oxide Ion Conductors

Werner Paulus, Helmut Schober, Stefan Eibl, Mark Johnson, Tanguy Berthier, Olivier Hernandez, Monica Ceretti, Marie Plazanet, Kazimierz Conder, and Carlo Lamberti

*J. Am. Chem. Soc.*, **2008**, 130 (47), 16080-16085 • DOI: 10.1021/ja806144a • Publication Date (Web): 06 November 2008



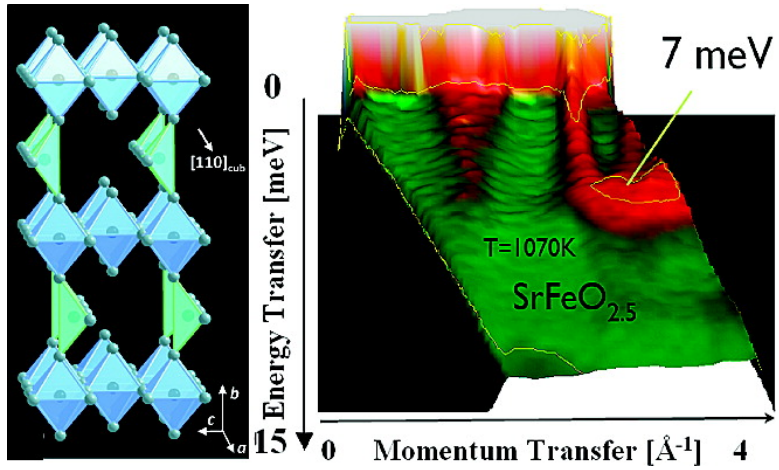


## More About This Article

Additional resources and features associated with this article are available within the HTML version:

- Supporting Information
- Access to high resolution figures
- Links to articles and content related to this article
- Copyright permission to reproduce figures and/or text from this article

View the Full Text HTML

J|A|C|S
ARTICLES

Published on Web 11/06/2008

# Lattice Dynamics To Trigger Low Temperature Oxygen Mobility in Solid Oxide Ion Conductors

Werner Paulus,*[,†] Helmut Schober,[‡] Stefan Eibl,[‡] Mark Johnson,[‡] Tanguy Berthier,[†,§] Olivier Hernandez,[†] Monica Ceretti,[†] Marie Plazanet,[‡,||] Kazimierz Conder,[⊥] and Carlo Lamberti[§]

*Sciences Chimiques de Rennes, UMR 6226 CNRS-Université de Rennes1, Inorganic Materials: Soft Chemistry and Reactivity of Solids, Campus de Beaulieu, F-35042 Rennes, France, Institut Laue-Langevin, BP 156 X, F-38042 Grenoble Cedex, France, Department of Inorganic, Physical and Materials Chemistry and NIS Center of Excellence, and INSTM "Centro di Riferimento", University of Turin, Italy, European Laboratory for Non-Linear Spectroscopy, University of Florence, Polo Scientifico, I-50019 Sesto-Fiorentin, Italy, and Laboratory for Developments and Methods, PSI, CH-5232 Villigen, PSI*

Received August 5, 2008; E-mail: werner.paulus@univ-rennes1.fr

***Abstract:*** $SrFeO_{2.5}$ and $SrCoO_{2.5}$ are able to intercalate oxygen in a reversible topotactic redox reaction already at room temperature to form the cubic perovskites $Sr(Fe,Co)O_3$, while $CaFeO_{2.5}$ can only be oxidized under extreme conditions. To explain this significant difference in low temperature oxygen mobility, we investigated the homologous $SrFeO_{2.5}$ and $CaFeO_{2.5}$ by temperature dependent oxygen isotope exchange as well as by inelastic neutron scattering (INS) studies, combined with *ab initio* (DFT) molecular dynamical calculations. From $^{18}O/^{16}O$ isotope exchange experiments we proved free oxygen mobility to be realized in $SrFeO_x$ already below 600 K. We have also evidence that low temperature oxygen mobility relies on the existence of specific, low energy lattice modes, which trigger and amplify oxygen mobility in solids. We interpret the INS data together with the DFT-based molecular dynamical simulation results on $SrFeO_{2.5}$ and $CaFeO_{2.5}$ in terms of an enhanced, phonon-assisted, low temperature oxygen diffusion for $SrFeO_{3-x}$ as a result of the strongly reduced Fe−O−Fe bond strength of the apical oxygen atoms in the $FeO_6$ octahedra along the stacking axis. This dynamically triggered phenomenon leads to an easy migration of the oxide ions into the open vacancy channels and vice versa. The decisive impact of lattice dynamics, giving rise to structural instabilities in oxygen deficient perovskites, especially with brownmillerite-type structure, is demonstrated, opening new concepts for the design and tailoring of low temperature oxygen ion conductors.

## 1. Introduction

The understanding of low temperature ion conductivity in solids is not only a key issue for the development of oxygen membranes and electrolytes in solid oxide fuel cells (SOFCs)[1] but concerns more generally fundamental aspects of diffusion processes. Concerning oxygen diffusion, there have been considerable efforts undertaken during the past decade to develop oxide membranes and electrolytes with high oxygen ion conductivity at moderate temperatures.[1−5] Thermodynamically, oxygen ion conduction in solids is described in terms of a thermally activated hopping process with ions jumping via vacant lattice sites.[6] Oxygen ions are doubly charged and have a rather large radius of about 1.4 Å. The energy barriers to overcome during the diffusion process are therefore high and normally require fairly elevated temperatures for diffusion to set in, even for structures possessing rather large vacancy sites. In this context, it is somehow surprising that there exist compounds into which oxygen ions can be intercalated reversibly at ambient temperature using "gentle" electrochemical methods or chemically by *chimie douce* conditions. The two structure types known today to undergo oxygen intercalation at ambient temperature belong either to the $K_2NiF_4$ structure, *e.g.* $La_2MO_{4+\delta}$ (M = Co, Ni, Cu)[7−10] or to the deficient perovskites and more specifically to the Brownmillerite-type

† UMR 6226 CNRS-Université de Rennes1.
‡ Institut Laue-Langevin.
§ University of Turin.
|| University of Florence.
⊥ Laboratory for Developments and Methods, PSI.

(1) Shao, Z. P.; Haile, S. M. *Nature* **2004**, *431*, 170–173.
(2) Minh, N. Q. *J. Am. Ceram. Soc.* **1993**, *76*, 563–588.
(3) Atkinson, A.; Barnett, S.; Gorte, R. J.; Irvine, J. T. S.; McEvoy, A. J.; Mogensen, M.; Singhal, S. C.; Vohs, J. *Nat. Mater.* **2004**, *3*, 17–27.
(4) Shao, Z. P.; Haile, S. M.; Ahn, J.; Ronney, P. D.; Zhan, Z. L.; Barnett, S. A. *Nature* **2005**, *435*, 795–798.
(5) Huang, Y. H.; Dass, R. I.; Xing, Z. L.; Goodenough, J. B. *Science* **2006**, *312*, 254–257.
(6) Goodenough, J. B. *Annu. Rev. Mater. Res.* **2003**, *33*, 91–128.
(7) Rudolf, P.; Paulus, W.; Schöllhorn, R. *Adv. Mater.* **1991**, *3*, 438–440.
(8) Paulus, W.; Heger, G.; Rudolf, P.; Schöllhorn, R. *Physica C* **1994**, *235*, 861–862.
(9) Alonso, J. A.; Martinez Lope, M. J.; Garcia Munoz, J. L.; Fernandez Diaz, M. T. *J. Phys.: Condens. Matter* **1997**, *9*, 6417–6426.
(10) Paulus, W.; Cousson, A.; Dhalenne, G.; Berthon, J.; Revcolevschi, A.; Hosoya, S.; Treutmann, W.; Heger, G.; Le Toquin, R. *Solid State Sci.* **2002**, *4*, 565–573.


10.1021/ja806144a CCC: $40.75 

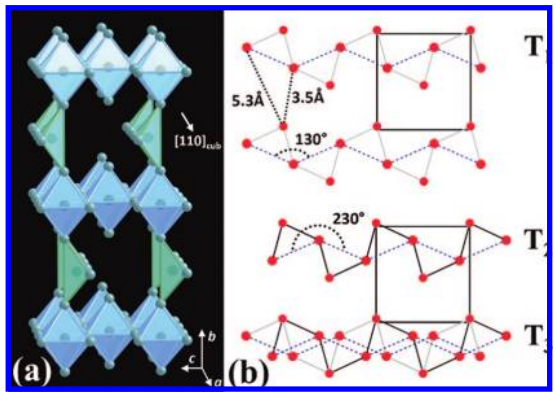


***Figure 1.*** (a) Idealized scheme of the Brownmillerite structure with 1D oxygen vacancy channels along [110] with respect to the cubic perovskite phase. $FeO_6$ octahedra and $FeO_4$ tetrahedra are reported in blue and green, respectively; Sr or Ca are omitted for clarity. In reality the tetrahedral chains show a zigzag arrangement as shown in part b ($T_1$ and $T_2$). Dynamical switching between $\mathbf{T_1}$ and $\mathbf{T_2}$ can trigger phonon assisted oxygen diffusion along the oxygen vacancy channel while the distances from the apical O to in plane O atoms vary between 3.5 and 5.3 Å. This disorder scenario is schematically represented as $\mathbf{T_3}$. The coordinate system (*a*, *b*, *c*) refers to the Brownmillerite structure in *Pnma*.

structure, such as $SrMO_{2.5}$ (M = Fe, Co).[11−13] In the case of $SrFeO_{3-x}$, the mixed ionic−electronic conductivity properties have already been investigated quantitatively both experimentally[14] and theoretically. Ma et al.[15,16] have investigated electrical transport properties in the system obtained by a partial substitution of Fe by Co.

In the search for improved oxygen ion conductors, the Brownmillerite structure has always played an important role and cation substituted $BaInO_{2.5}$ may be regarded as the most prominent example of this series.[17,18] This might be strongly related to the peculiarities of the Brownmillerite structure, consisting of alternating octahedral and tetrahedral layers and notably the presence of 1D ordered vacancy channels in the tetrahedral layers, which have themselves an average diameter of about 3.5 Å (see Figure 1). It has been shown recently that in the case of the isostructural $SrCoO_{2.5}$ and $SrFeO_{2.5}$ these channels can be filled up completely already at room temperature (RT) to form the cubic perovskite $Sr(Co,Fe)O_3$[13,19] in a reversible topotactic redox reaction,[20] *i.e.* by electrochemical oxidation. This is naturally in strong contradiction to the current understanding of oxygen ion conduction in solid oxides, which is believed to require at least temperatures above 900 K. With respect to $Sr(Fe,Co)O_{2.5}$ it appears then surprising that the isostructural $CaFeO_{2.5}$ requires high oxygen pressure at elevated temperature to form $CaFeO_3$ and that soft chemistry methods at ambient conditions fail in this case.[21] Comparison of the Ca and Sr homologous Brownmillerite phases is therefore supposed to deliver the *conditio sine qua non* required for low temperature oxygen ion mobility.

## 2. Experimental Details and Methods

The starting powders were prepared by thoroughly grinding stoichiometric quantities of high purity $SrCO_3$ or $CaCO_3$ (99.95%) and $Fe_2O_3$ (99.99%) in the presence of acetone, allowing better intermixture to give a total amount of about 5 g. After drying in ambient atmosphere, this mixture was first heated in air at 1300 K for 24 h. After furnace cooling, the resultant powder was manually ground and pressed into pellets of 13 mm in diameter and 1 g in weight, which were again heated in air for 24 h at 1300 K followed by a subsequent annealing at 1500 K for 24 h and quenching the pellets from 1500 K into liquid nitrogen. This procedure was repeated twice. In the case of the Ca phase, this procedure already yields stoichiometric $CaFeO_{2.5}$. In order to obtain stoichiometric $SrFeO_{2.5}$, the as obtained pellets were reheated for 6 h at 1300 K in a quartz tube under dynamic vacuum and were cooled down by placing the whole quartz tube in liquid nitrogen. The obtained products were identified by X-ray diffraction to be stoichiometric $CaFeO_{2.5}$ and $SrFeO_{2.5}$ (see Figure S1). Thermogravimetric measurements have been carried out on a NETSCH thermobalance Jupiter STA 449C, equipped with a PFEIFFER VACUUM ThermoStar mass spectrometer.

DFT calculations have been performed using the VASP code.[22] We used the PBE functional, PAW pseudopotentials, a *k*-point spacing of 0.1 $Å^{-1}$, and a plane wave energy cutoff of 270 eV. Molecular dynamics simulations were performed with VASP for a supercell composed of two unit cells in the direction of the tetrahedral chains. The phonon calculations were performed using the direct method as implemented in the PHONON code.[23] In this case, an approximately square-based [2,1,2] supercell was used. Shell-model calculations were performed with GULP.[24]

The inelastic neutron scattering (INS) measurements were performed on the cold neutron time-of-flight spectrometer IN6 of the ILL. The incident wavelength was 4.12 Å, and neutrons were detected over scattering angles from 13° to 114° 2Θ.

We used a slightly inelastic focusing ($E_{focus}$ = 2.7 meV) to improve resolution at large energy transfers in up-scattering (neutron energy gain mode). The raw data were corrected for empty container scattering and normalized to a vanadium standard. The spectra thus obtained were converted into generalized phonon density of states (GDOS) $G(\omega)$ using the incoherent approximation. Multiphonon corrections were performed self-consistently.[25] The neutron-weighted GDOS is related to the true partial phonon density of states $g_i(\omega)$ ($i$ = Sr, Ca, Fe, and O) according to

$$G(\omega) = \frac{\sum_{i=(Sr,Ca),Fe,O} (c_i\sigma_i/m_i)\cdot g_i(\omega)}{\sum_{i=(Sr,Ca),Fe,O} (c_i\sigma_i/m_i)}$$

where $c_i$ indicates the concentration, $\sigma_i$ is the total bound scattering cross section for atoms $i$, and $m_i$ is its mass. Consequently, $G(\omega)$ is related to the true total phonon density of states $g(\omega)$ by a

(11) Takeda, Y.; Kanno, R.; Takada, T.; Yamamoto, O.; Takano, M.; Bando, Y. *Z. Anorg. Allg. Chem.* **1986**, *540*, 259–270.
(12) Nemudry, A.; Rudolf, P.; Schöllhorn, R. *Chem. Mater.* **1996**, *8*, 2232–2238.
(13) Le Toquin, R.; Paulus, W.; Cousson, A.; Prestipino, C.; Lamberti, C. *J. Am. Chem. Soc.* **2006**, *128*, 13161–13174.
(14) Patrakeev, M. V.; Leonidov, I. A.; Kozhevnikov, V. L.; Kharton, V. *Solid State Sci.* **2004**, *6*, 907–913.
(15) Ma, B.; Balachandran, U.; Park, J. H.; Segre, C. U. *J. Electrochem. Soc.* **1996**, *143*, 1736–1744.
(16) Ma, B.; Balachandran, U.; Park, J. H.; Segre, C. U. *Solid State Ionics* **1996**, *83*, 65–71.
(17) Goodenough, J. B.; Ruizdiaz, J. E.; Zhen, Y. S. *Solid State Ionics* **1990**, *44*, 21–31.
(18) Goodenough, J. B.; Manthiram, A.; Kuo, J. F. *Mater. Chem. Phys.* **1993**, *35*, 221–224.
(19) Nemudry, A.; Weiss, P.; Gainutdinov, I.; Boldyrev, V.; Schöllhorn, R. *Chem. Mater.* **1998**, *10*, 2403–2411.
(20) Schaak, R. E.; Mallouk, T. E. *Chem. Mater.* **2002**, *14*, 1455–1471.
(21) Takeda, Y.; Naka, S.; Takano, M.; Shinjo, T.; Takada, T.; Shimada, M. *Mater. Res. Bull.* **1978**, *13*, 61–66.
(22) Kresse, G.; Furthmuller, J. *Phys. Rev. B* **1996**, *54*, 11169–11186.
(23) Parlinski, K. Calculation of phonon dispersion curves by the direct method. In *Neutrons and numerical methods*; Johnson, M. R., Kearley, G. J., Büttner, H. G., Ed.; AIP Conference Proceedings; 1999; Vol. 479, pp 121−126.
(24) Gale, J. D.; Rohl, A. L. *Mol. Simul.* **2003**, *29*, 291–341.
(25) Schober, H.; Tölle, A.; Renker, B.; Heid, R.; Gompf, F. *Phys. Rev. B* **1997**, *56*, 5937–5950.

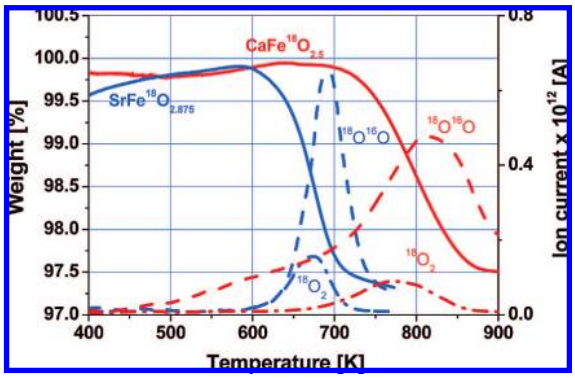


***Figure 2.*** Thermogravimetric−mass spectroscopic study of $SrFe^{18}O_{2.875}$ (blue lines) and $CaFe^{18}O_{2.5}$ (red lines), both enriched by about 85% in $^{18}O$, carried out in an $^{16}O_2$ atmosphere using a heating rate of 5 K/min. The instant changes of the mass of about 2.5%, observed for $SrFeO_{2.875}$ slightly above 600 K, correspond to the entire transformation of $SrFe^{18}O_{2.875}$ to $SrFe^{16}O_{2.875}$. A mass change of 3% would be expected in the case of a totally enriched sample. We note that the transformation is completed in 20 min, indicating a rapid oxygen isotope exchange and mobility. The dashed-dotted and dashed lines correspond to the simultaneously measured $^{18}O-^{18}O$ and $^{18}O-^{16}O$ mass signals (ion current), respectively. The maximum of the $^{18}O-^{18}O$ signal is slightly shifted toward lower temperatures with respect to the $^{18}O-^{16}O$ signal, as the pure recombination of $^{18}O$ oxygen atoms is more probable in the beginning of the isotope exchange reaction. The oxygen isotope exchange for $CaFeO_{2.5}$, which itself remains stable in oxygen stoichiometry at least up to 1300 K, sets in at higher temperature, about 750 K. Qualitatively, oxygen mobility can be estimated to be much slower in $CaFeO_{2.5}$ compared to $SrFeO_{2.875}$, not only because of the difference in temperature where oxygen diffusion sets in but also as the temperature interval for complete isotope exchange is much narrower for $SrFeO_{2.875}$.

frequency-dependent factor $f(\omega) = g(\omega)/G(\omega)$, which has no simple expression but can be determined from the lattice dynamical calculations.

## 3. Results and Discussion

The high oxygen mobility in $SrFeO_x$ is equally demonstrated to occur even without any external solicitation such as the applied electrochemical potential cited above. Thermogravimetric investigations of $^{18}O$ enriched $SrFeO_{2.875}$ in an $^{16}O_2$ atmosphere allow an easy access of the exchange equilibria of the different oxygen isotopes as a function of temperature, and thus oxygen mobility at least on a qualitative level. Following this, we studied oxygen isotope exchange behavior (see Figure 2) for $CaFe^{18}O_{2.5}$ and $SrFe^{18}O_{2.875}$. Since $CaFeO_{2.5}$ is stoichiometric with respect to its oxygen content at least up to 1300 K, it can be directly used for the isotope exchange experiments. This is no longer true for $SrFeO_{2.5}$, which takes up oxygen already below 600 K, while transforming into $SrFeO_{2.875}$, and which itself does not vary its oxygen stoichiometry between RT and 750 K. When heating $SrFe^{18}O_{2.875}$ in an $^{16}O_2$ atmosphere with a heating rate of 5 K/min, a mass decrease of about 2.5% is observed, setting in at already 600 K. This mass difference can be explained by an exchange of all $^{18}O$ atoms in $SrFe^{18}O_{2.875}$, thus forming $SrFe^{16}O_{2.875}$. The exchange reaction is completed in less than 20 min, *i.e.* in a temperature range of about 100 K. We notice that $SrFeO_{2.875}$ shows a deficient Perovskite structure with cubic symmetry above 600 K, thus rendering all oxygen atoms crystallographically equivalent. Under the same dynamic reaction conditions (heating rate 5 K/min), $CaFeO_{2.5}$ also shows an oxygen isotope exchange reaction, but the reaction sets in at higher temperature (>750 K) and the reaction is completed in a temperature range of about 200 K, which is nearly twice the value compared to the case of $SrFeO_{2.875}$.

From a structural point of view, $CaFeO_{2.5}$ and $SrFeO_{2.5}$ mainly differ in the elongation of the *b*-axis, *i.e.* the stacking-axis of octahedral and tetrahedral layers (see Figure 1 and Table S1), which is, at RT, significantly shorter for the Ca phase (14.77 vs 15.57 Å). Structural differences also arise from the order−disorder phenomena concerning the $FeO_4$ tetrahedral chains. $CaFeO_{2.5}$, crystallizing in the *Pnma* space group, shows an ordered tetrahedral layer, while it is disordered for $SrFeO_{2.5}$. The disorder is best described in the *Imma* space group, implying split positions of iron and oxygen atoms along the tetrahedral chain (see Figure 1 and Figures S1 and S2). This disorder is equivalent to a superposition of the two $FeO_4$ chain formations given in Figure 1b and, as will be shown later, is of dynamical origin already at and above RT. This type of structural disorder is unique and only present in Brownmillerite-type frameworks[13] (Figure 1). The disorder scheme is a crucial point toward a possible understanding of oxygen diffusion along the 1D vacancy channels, as we may postulate that the dynamically disordered $MO_4$ chains may behave as *internal interfaces*, allowing a permanent variation of the apical to in plane oxygen distances of adjacent $MO_4$ chains between 3.5 and 5.3 Å (Figure 1b). For an oxygen atom, moving along the vacancy channel, the permanent switching mode would behave like a gate, which opens and closes with the switching frequency, thus pushing the oxygen atoms through. Consequently, the different oxygen intercalation behavior found for $CaFeO_{2.5}$ and $SrFeO_{2.5}$ at RT should be a direct response of their different lattice dynamics and ordering state.

To explore the lattice dynamics of $(Sr,Ca)FeO_{2.5}$, we have undertaken inelastic neutron scattering (INS) experiments on the IN6 time-of-flight spectrometer (ILL Grenoble) at different temperatures; the results are summarized in Figure 3a. As the two compounds show slightly different structures with different space groups at RT, their lattice dynamics are therefore not directly comparable. However, $CaFeO_{2.5}$ undergoes a phase transition on heating around 973 K,[26] approaching on an average scale the structure of $SrFeO_{2.5}$ at RT.[27]

From the INS spectra, significant differences are observed at RT for the low energy excitations, situated at 7 and 12 meV for $SrFeO_{2.5}$ and $CaFeO_{2.5}$ respectively. The low energy peak position remains almost invariant with temperature for the Sr compound but undergoes a significant red shift to 9 meV for the Ca homologue at 1073 K (Figure 3a). Structural changes associated with this phase transition in $CaFeO_{2.5}$ mainly concern the increase of disorder of the $FeO_4$ tetrahedra chains, indicating that the 12 to 9 meV shift involves lattice modes, specifically related to the tetrahedral layers.

State-of-the-art calculations based on *ab initio* (DFT) molecular dynamics (Supplementary Figure S3) allowed extraction of remarkable peculiarities in the lattice dynamics for both compounds. First, we were able to simulate that the square arrangements of oxygen atoms in the $FeO_6$ octahedra present a very stable configuration for both $SrFeO_{2.5}$ and $CaFeO_{2.5}$. A single defect, artificially created by arbitrarily displacing an equatorial oxygen ion, heals within a few picoseconds at simulation temperatures of about 750 K. The situation is

(26) Berastegui, P.; Eriksson, S. G.; Hull, S. *Mater. Res. Bull.* **1999**, *34*, 303–314.
(27) Krüger, H.; Kahlenberg, V. *Acta Crystallogr., Sect. B: Struct. Sci.* **2005**, *61*, 656–662.

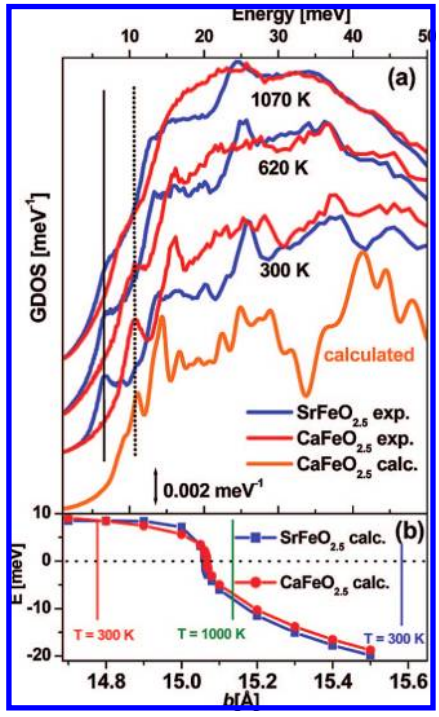


***Figure 3.*** (a) Experimental GDOS of $SrFeO_{2.5}$ (blue) and $CaFeO_{2.5}$ (red) obtained from INS performed on the IN6 spectrometer at the ILL (Grenoble, France) at different temperatures vertically shifted for clarity: 300 K (bottom), 620 K (middle), and 1070 K (top). The orange spectrum reports the calculated DOS for $CaFeO_{2.5}$ at 0 K. The low energy mode was found at 7 meV for $SrFeO_{2.5}$ independent of the temperature (vertical solid line); for $CaFeO_{2.5}$, below the *Pnma* → *Imma* phase transition (300 and 620 K), it appears at 12 meV (vertical dotted line), being softened to 9 meV above the transition (1070 K). (b) Dependence of the computed soft mode energy at the Γ point of $SrFeO_{2.5}$ (blue) and $CaFeO_{2.5}$ (red) as a function of the *b*-lattice parameter, *i.e.* the stacking axis of the octahedral and tetrahedral layers. Independent of the A cation (Sr, blue, or Ca, red points), the critical value of the *b* axis where the frequency of the mode becomes negative, reflecting structural instabilities, is around 15.05 Å. The experimental lattice parameters at RT for $SrFeO_{2.5}$ ($b = 15.57$ Å) and $CaFeO_{2.5}$ ($b = 14.77$ Å) are given as blue and red vertical lines, respectively. We equally indicate the value of $b = 15.13$ Å observed for $CaFeO_{2.5}$ at 1000 K[26] as a green vertical line.

completely different regarding the apical oxygen atoms: while trapped at RT in $CaFeO_{2.5}$, they show considerable displacements for $SrFeO_{2.5}$. The potential of the apical oxygen atoms is mainly determined by the Fe−O bond length, with the bonding character being strongly covalent. If now the apical oxygen atom gets sufficiently far away from its equilibrium position, our simulations show that it is even able to escape into the vacancy channels of the tetrahedral layer, leaving behind a square pyramid and a reoriented tetrahedron (see Figure 4a−e and *vide infra* Figure 6). We note that $FeO_5$ square pyramids are energetically stable structural units and are found for example in $Sr_3Fe_2O_6$[28] or in $SrFeO_{2.875}$.[29] The DFT simulations also confirm pronounced lattice dynamics for the tetrahedral chains of $SrFeO_{2.5}$, *i.e.* a marked zigzag to zagzig switching behavior on a picosecond time scale at RT, as indicated in Figure 1b. This switching is strongly amplified toward higher temperatures. This type of lattice dynamics is entirely absent for $CaFeO_{2.5}$ at ambient temperature and sets in at higher temperatures only (1070 K), as evident from Figure 3a.

The oxygen diffusion pathways emerging from these DFT simulations are graphically illustrated in Figure 4d and e as the

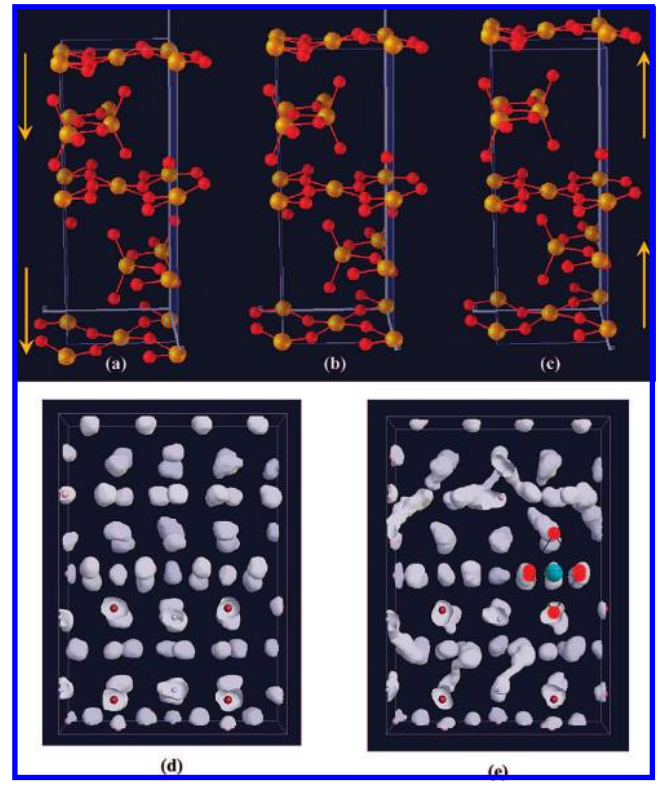


***Figure 4.*** Representation of the lattice mode, observed at 12 meV for $CaFeO_{2.5}$, leading to the instability of the apical oxygen position. This mode involves a unidirectional shift, as indicated by the orange arrows of the upper and lower octahedral (at $y = 0$) and tetrahedral layers (at $y = \pm 1/4$), while the position of the octahedral layer situated at $y = 1/2$ remains almost constant. Part (b) corresponds to the equilibrium position, while parts (a) and (c) show the extreme positions of the dynamically displaced layers. Envelopes of trajectories followed by O atoms along 10 ps *ab initio* molecular dynamics (350 K) for (d) $CaFeO_{2.5}$ and (e) $SrFeO_{2.5}$. In the case of $CaFeO_{2.5}$, O atoms vibrate around a well-defined crystallographic position, while, in $SrFeO_{2.5}$, the migration of the apical O atoms to the vacant in-plane tetrahedral sites is observed. Superimposed in part (e) is one $FeO_6$ octahedra (oxygen atoms in red and the iron atom in green).

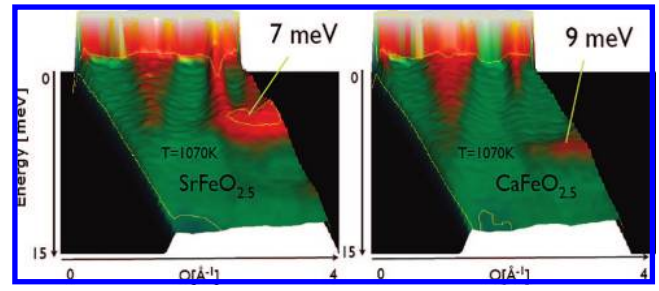


***Figure 5.*** Scattering function $S(Q,\omega)$ for $SrFeO_{2.5}$ (left) and $CaFeO_{2.5}$ (right), collected on IN6 (ILL, Grenoble) at 1070 K. In both cases, the acoustic phonons emerging from the Bragg peaks and the dominating low-frequency band of optic vibrations become evident. While in the case of $CaFeO_{2.5}$ the optic band is nicely separated from the acoustic phonon intensities, it merges with those in the case of $SrFeO_{2.5}$. This can be explained by the lower frequency of that band (7 meV for $SrFeO_{2.5}$ and 9 meV for $CaFeO_{2.5}$). Closer inspection of the region near the elastic line reveals that the intensity in $CaFeO_{2.5}$ around 2.25 Å$^{-1}$ still has phonon character, *i.e.* $S(Q,\omega)$ is constant as a function of $\omega$, while a quasi-elastic contribution in $SrFeO_{2.5}$ is observed, indicating relaxation motion.

(28) Dann, S. E.; Weller, M. T.; Currie, D. B. *J. Solid State Chem.* **1992**, *97*, 179–185.
(29) Hodges, J. P.; Short, S.; Jorgensen, J. D.; Xiong, X.; Dabrowski, B.; Mini, S. M.; Kimball, C. W. *J. Solid State Chem.* **2000**, *151*, 190–209.

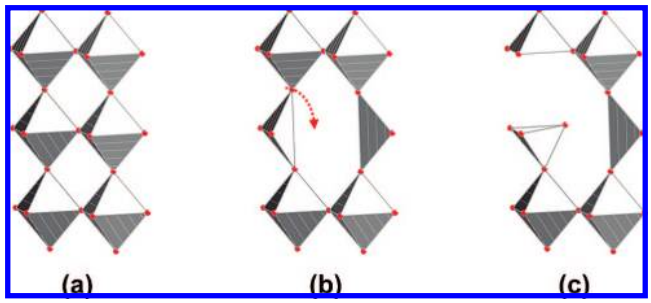


***Figure 6.*** Structure schemes of (a) the Perovskite and (b) the Brownmillerite framework. Part (c) presents the intermediate state after the diffusion of an apical oxygen atom to a vacant lattice site in the tetrahedral layer (see red arrow), yielding locally a $FeO_5$ square pyramid and a newly formed $FeO_4$ tetrahedron.

envelopes of particle trajectories which were summed up over a time period of 10 ps for a given temperature of 350 K. In the case of $SrFeO_{2.5}$ (Figure 4e), the formation of "wormholes" becomes evident, indicating the migration of the apical oxygen atoms into the vacancy channels. For $CaFeO_{2.5}$ (Figure 4d) no evidence for oxygen diffusion could be derived from these simulations. The combination of oxygen migration based on structural instabilities together with the dynamic fluctuations of the tetrahedral chains may therefore be an important prerequisite to allow low temperature oxygen ion mobility in solids, at least for those with Brownmillerite-type structure.

Calculating the phonon dispersion curves is straightforward for $CaFeO_{2.5}$, and the calculated density-of-states (DOS) compares very nicely with the INS data (see orange curve in Figure 3a and Figure S3). Analysis of the displacement vectors shows that the 12 meV band contains specific motions concerning iron and apical oxygen atoms of the $FeO_6$ octahedron along the *b* axis (see Figure 4a−c). The same calculations for $SrFeO_{2.5}$, assuming an ordered $FeO_4$ tetrahedra zigzag chain arrangement, yield negative phonon branches (Figure 3b), regardless of the considered space group, *Pnma* or *I2mb*. The disordered structure model in *Imma* cannot be directly used for DFT calculations due to the split positions of iron and oxygen. The displacement vectors corresponding to these negative frequencies strongly resemble those of the low-frequency band in $CaFeO_{2.5}$. They dynamically separate one of the apical oxygen atoms from the rest of the octahedron, causing a structural instability consistent with a shallow potential for oxygen diffusion pathways following the "wormhole" scenario discussed above; see Figure 4e. Using a shell model approach, it is possible to demonstrate that this structural instability strongly depends on the lattice parameter of the *b*-axis, *i.e.* the stacking direction. Reducing the *b*-axis parameter, *i.e.* going from $SrFeO_{2.5}$ to $CaFeO_{2.5}$, goes along with a stabilization of the apical oxygen position, hindering naturally any oxygen mobility (see Figure 3b).

The importance of the low-frequency vibrations for the oxygen mobility is equally demonstrated by the high-temperature ($T = 1070$ K) neutron scattering results on $SrFeO_{2.5}$. As seen from the quasi-elastic spectra (see Figure 5), the optical band merges with the acoustic phonons emerging from the Bragg peak position. Quasi-elastic scattering around the Bragg peak indicates fast oxygen diffusion. We note that the merging of bands and the quasi-elastic scattering are absent in $CaFeO_{2.5}$ (Figure 5); that is, the diffusion is too slow to enter the time window of IN6. This underlines the difference of the two systems even in the high-temperature regime.

In the case of $SrFeO_{2.5}$, the local instability of the apical oxygen atoms suggests that its structure is better described as

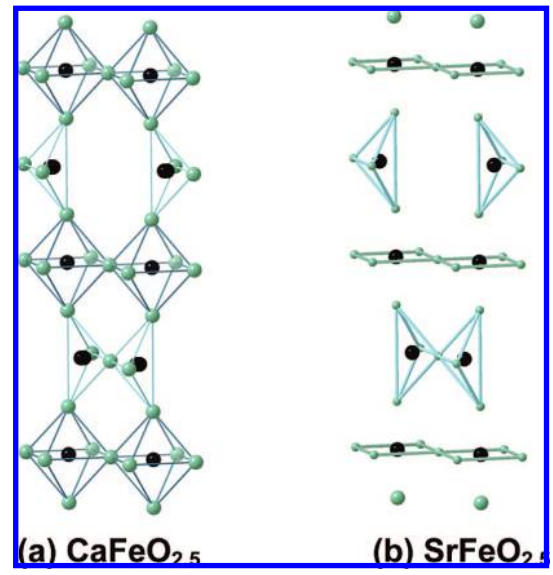


***Figure 7.*** Schematic structures of $CaFeO_{2.5}$ and $SrFeO_{2.5}$. Black and gray spheres represent Fe and O atoms, respectively; Sr and Ca are omitted for clarity. (a) For $CaFeO_{2.5}$ the classical description of the Brownmillerite framework, *i.e.* the sequence of alternating octahedra and tetrahedra layers, is outlined. (b) For $SrFeO_{2.5}$, this picture has to be reconsidered, as the apical oxygen atoms are no longer associated with the $FeO_6$ octahedra layers (see text) and have to be mainly accounted to the $FeO_4$ tetrahedra chains. In this way, $SrFeO_{2.5}$ yields in a sequence of square planar $FeO_4$ layers, alternating with layers of $FeO_4$ tetrahedra chains. Note that $SrFeO_2$ with infinite $(FeO_2)_\infty$ layer structure and $Sr_3Fe_2O_5$ showing a square planar $FeO_4$ coordination have recently been reported to be stable compounds.[31,32]

a sequence of infinite $(FeO_2)_\infty$ layers containing square planar $FeO_4$ units, alternating with $FeO_4$ tetrahedra layers, rather than the classical description of alternating octahedral and tetrahedral layers (see Figure 7). From a crystal-chemistry point of view, the apical oxygen atoms should thus be regarded as attached to the $FeO_4$ tetrahedra only. Note that $SrFeO_2$ with an infinite $(FeO_2)_\infty$ layer structure showing a square planar $FeO_4$ coordination has recently been reported.[30−32] Brownmillerite frameworks with large A-cations such as Sr or Ba, serving as spacers, thus dispose on structurally "autonomous" $FeO_4$ tetrahedral chains (see Figure 1b). The latter may then be regarded as dynamically decoupled from the separating infinite layers, allowing possible "eigen"-fluctuations of the tetrahedral chains described above. It is questionable whether the dynamical instability of the apical oxygen atoms and the related oxygen diffusion mechanism cause the specific switching behavior of the $FeO_4$ zigzag chains or *vice versa*.

## 4. Summary, Conclusions, and New Perspectives

This work concerns the fundamental understanding of low temperature oxygen mobility in deficient Perovskite frameworks, achieved combining temperature dependent $^{18}O/^{16}O$ isotope exchange experiments and INS with *ab initio* (DFT) molecular dynamical calculation. The particular interference of dynamically triggered parameters clearly demonstrates the decisive role

(30) Hayward, M. A.; Rosseinsky, M. J. *Nature* **2007**, *450*, 960–961.
(31) Tsujimoto, Y.; Tassel, C.; Hayashi, N.; Watanabe, T.; Kageyama, H.; Yoshimura, K.; Takano, M.; Ceretti, M.; Ritter, C.; Paulus, W. *Nature* **2007**, *450*, 1062–1067.
(32) Kageyama, H.; Wataabe, T.; Tsujimoto, Y.; Kitada, A.; Sumida, Y.; Kanamori, K.; Yoshimura, K.; Hayashi, N.; Muranaka, S.; Takano, M.; Ceretti, M.; Paulus, W.; Ritter, C.; André, G. *Angew. Chem., Int. Ed.* **2008**, *47*, 5740–5745.

that lattice dynamics, together with geometrical considerations, can play, to enable and to reinforce oxygen ion mobility in solid oxides. This allowed us to get the first insights toward a better microscopic understanding of low temperature oxygen diffusion mechanisms, different from the classical one and the thermally activated hopping one.[6]

Deviation of ion conductivity from the pure Arrhenius behavior had already been described by the Vogel−Tamman−Fucher (VTF)[33−35] and Williams−Landel−Ferry (WLF)[36] equations. These descriptions, based on phenomenological approaches, assume faster relaxation processes induced by thermal motion, without providing a microscopic interpretation of enhanced low-temperature ion conductivity. Anomalies have been reported *e.g.* for polymer electrolytes,[37] silver conducting AgI composite glasses,[38] and crystallized chalcogenides.[39] Ionic transport described by the VTF equation is much less common in oxides, but it has already been reported for lithium diffusion in $La_{2/3-x}Li_{3x}TiO_3$ solid solutions ($0.07 \leq x \leq 0.13$)[40] and for oxygen diffusion in $La_2Mo_{2-y}W_yO_9$ ($y \leq 1.4$).[41]

Coming back to the present case, the oxygen diffusion pathway and exchange mechanism between adjacent $FeO_x$ ($x = 4, 5, 6$) polyhedra highly resembles the Grotthus proton diffusion mechanism in water,[42] apart from two main differences: compared to the "tunnelling" of protons, the time scale for oxygen diffusion is reduced from femto- to picoseconds and an important driving force for oxygen diffusion must be attributed to specific lattice modes. In addition to lattice dynamical aspects, oxygen diffusion in solids should get reinforced, whenever rapid fluctuations of the coordination sphere and valence states of the transition metal cations can be achieved. Fe is in this context a remarkable chemical chameleon, as it is able to easily change its coordination from square-planar to tetrahedral, to square pyramidal, and, finally, to octahedral, when going successively from $SrFeO_2$ to $SrFeO_{2.5}$, $SrFeO_{2.875}$, and $SrFeO_3$.[29−31] A balanced interplay between geometrical considerations, mainly related to the large $Sr^{2+}$ ions, accompanied by easy fluctuations in the $FeO_x$ coordination and associated valence state, yields together with lattice dynamical considerations a promising basis to equally explain oxygen mobility for oxygen deficient perovskites with almost cubic symmetry.

Probing soft phonon modes to be a prerequisite for low temperature oxygen mobility seem to be a promising concept which appears to be more generally applicable than in Brownmillerite frameworks only, where oxygen diffusion occurs via vacant regular lattice sites. Prominent examples showing oxygen diffusion via interstitial lattice sites emanate from the $K_2NiF_4$ family, *i.e.* $La_2NiO_{4+x}$[43] or $La_2CoO_{4+x}$.[44] Also in these compounds instabilities of the apical oxygen atoms, expressed as strong structural displacements, have been observed via high resolution neutron diffraction[10,44] and could have also been confirmed by DFT calculations.[45]

It is clear that the fundamental understanding of oxygen ion mobility in solid oxides at moderate temperature requires new mechanisms, different from the thermally activated hopping process, as the energy barriers for oxygen diffusion cannot be overcome at ambient temperature. The concept to realize oxygen diffusion via lattice instabilities and dynamically triggered internal interfaces, as realized in Brownmillerites, offers a new dimension not only to design and to tune fast oxygen ion conductors in solids, but also more generally for the understanding of low temperature solid state reactivity with a special accent on reversible battery systems.

**Acknowledgment.** This research project has been partially supported by Rennes Métropole, the Région Bretagne, the French Ministry for Education and Research (CPER 2000-06), and the NIS centre of excellence (Torino, Italy). The financial support from ILL to allow the travel to and the stay in Grenoble during INS measurements is gratefully acknowledged. This work represents a collaboration inside the MaMaSELF European Master in Materials Science (http://etudes.univ-rennes1.fr/mamaself).

**Supporting Information Available:** Lattice parameters, X-ray diffraction patterns, and PDOS of $(Ca,Sr)FeO_{2.5}$, and representations of the chains of $FeO_4$ tetrahedra. This material is available free of charge via the Internet at http://pubs.acs.org.

JA806144A

(33) Vogel, H. *Phys. Z.* **1921**, *22*, 645–646.
(34) Tammann, G.; Hesse, W. *Z. Anorg. Allg. Chem.* **1926**, *156*, 245–257.
(35) Fulcher, G. S. *J. Am. Ceram. Soc.* **1925**, *8*, 339–355.
(36) Williams, M. L.; Landel, R. F.; Ferry, J. D. *J. Am. Chem. Soc.* **1955**, *77*, 3701–3707.
(37) Gray, F.; Armaud, M. Polymer Electrolytes. In *Handbook of Battery Materials*; Besenhard, J. O., Ed.; Wiley-VCH: Weinheim, 1999; pp 499−523.
(38) Kuwata, N.; Saito, T.; Tatsumisago, M.; Minami, T.; Kawamura, J. *Solid State Ionics* **2004**, *175*, 679–682.
(39) Ribes, M.; Taillades, G.; Pradel, A. *Solid State Ionics* **1998**, *105*, 159–165.
(40) Bohnke, O.; Bohnke, C.; Fourquet, J. L. *Solid State Ionics* **1996**, *91*, 21–31.
(41) Georges, S.; Bohnke, O.; Goutenoire, F.; Laligant, Y.; Fouletier, J.; Lacorre, P. *Solid State Ionics* **2006**, *177*, 1715–1720.
(42) de Grotthus, C. J. T. *Ann. Chim.* **1806**, *LVIII*, 54–74.
(43) Pintschovius, L.; Bassat, J. M.; Odier, P.; Gervais, F.; Chevrier, G.; Reichardt, W.; Gompf, F. *Phys. Rev. B* **1989**, *40*, 2229–2238.
(44) Le Toquin, R.; Paulus, W.; Cousson, A.; Dhalenne, G.; Revcolevschi, A. *Physica B* **2004**, *350*, e269–e272.
(45) Frayret, C.; Villesuzanne, A.; Pouchard, M. *Chem. Mater.* **2005**, *17*, 6538–6544.